Ultrashort pulsed squeezing by optical parametric amplification

M. J. Werner*
Department of Physics, University of Queensland, St. Lucia, 4072 Brisbane, Australia

M. G. Raymer and M. Beck†
Department of Physics, University of Oregon, Eugene, Oregon 97403

P. D. Drummond‡
Department of Physics, University of Waikato, Hamilton, New Zealand

(Received 18 January 1995)

We investigate temporal effects in pulsed squeezing by parametric amplification, including effects of group-velocity dispersion. Our calculations show that the local oscillator pulse used to detect the squeezed field cannot be made shorter than the inverse phase-matching bandwidth of the generation process without degrading the amount of squeezing detected. This result generalizes an earlier result that showed that in the absence of dispersion, the local oscillator pulse duration should approach zero for optimum squeezing detection. We further show that by using local oscillator amplitude and phase pulse shaping it should be possible to achieve more than 20 dB of detectable quadrature squeezing. This is applicable where it is possible to neglect transverse spatial dimensions and diffraction, such as in a waveguide. We derive the s-parametrized quasiprobability evolution equation for the traveling-wave parametric amplifier. As the Wigner representation results in third-order derivatives, we also use the positive-P representation as an exact representation with equivalent Ito stochastic differential equations. This allows us to compare approximate — but easily simulated — Wigner representation results with those using the positive-P representation.

PACS number(s): 42.50.Dv, 42.65.Ky

I. INTRODUCTION

It has been an aim for some time to produce a source of broadband, highly squeezed light. Following the first demonstrations of continuous-wave quadrature squeezing of light fields via four-wave mixing [1], parametric oscillation [2], and the Kerr effect [3], attention turned to experiments using pulsed interactions as a possible method to obtain wideband squeezing with large numbers of photons per mode [4–8]. The traveling-wave optical parametric amplifier (OPA) has been used as a relatively simple source of pulsed squeezed light. By propagating a collimated pulse of intense laser light, with frequency ω_2, through a medium with a $\chi^{(2)}$ optical nonlinearity, light near the subharmonic frequency ($\omega_1 = \omega_2/2$) can be spontaneously generated by parametric down-conversion. When phase-matching conditions are met and if the laser field is intense enough, optical parametric amplification occurs during a single pass through the medium. This converts the fundamental frequency to wideband, tunable light. It has been shown that this light is quadrature squeezed, leading to noise below the shot-noise level in homodyne detection [4–6].

This paper will concentrate on the temporal and dispersive effects involved in pulsed squeezing and will consider both a typical experimental configuration and more idealized situations to demonstrate the possible direction of future experiments. Here we consider only temporal effects, as would be appropriate for a parametric waveguide. Experimental results on quadrature squeezing in $\chi^{(2)}$ waveguides have recently been reported [9]. In a future paper we plan to include the spatial effects in a nonlinear dispersive medium that are important for typical bulk crystal experiments. We emphasize the Wigner representation as an efficient computational approach for large photon numbers. Use of the Wigner representation for squeezing in traveling-wave parametric amplifiers has been suggested previously by Kupiszewska and Rzążewski [10].

We also develop a rather general analysis for realistic pulsed squeezing experiments in one-dimensional propagation systems. We confirm that the local oscillator pulse used to detect the squeezed field cannot be made shorter than the inverse phase-matching bandwidth of the generation process without degrading the amount of squeezing detected [11]. This result generalizes that of Yurke and co-workers [12], which showed that in the absence of dispersion, the local oscillator pulse duration should approach zero for optimum squeezing detection. Using local oscillator pulse shaping, it should be possible to achieve more than 20 dB of detectable quadrature squeezing, provided that linear losses are negligible.

An analysis of pulsed squeezing assuming perfect phase matching and no medium dispersion was given by Yurke and co-workers [12]. The assumptions of perfect phase matching over an infinite bandwidth and no pump depletion simplify the problem considerably and provide useful solutions for a limiting case. Their conclusion was that the duration of the local oscillator (LO) pulse used for

*Present address: NTT Basic Research Laboratories, 3-1 Morinosato-Wakamiya, Atsugi-city, Kanagawa-pref, 243-01, Japan.

†Present address: Department of Physics, Reed College, Portland, OR 97202.

‡Present address: Department of Physics, University of Queensland, St. Lucia 4072, Brisbane, Australia.

homodyne detection should be shorter than the duration of the pump pulse. In fact, the prediction dictates that the shorter the local oscillator pulse, the stronger the detected squeezing. Also, they indicate that the technique of using a much shorter local oscillator pulse would allow detection of squeezing variations along the signal pulse envelope. They suggest that pulse compression techniques on the local oscillator or passing the pump pulse through a cavity could be used to achieve the desired shorter local oscillator, given the fact that the pump field is derived by second-harmonic generation of the source from which the local oscillator is taken.

We note that pump pulse dispersion and group-velocity mismatch both temporally broaden the down-converted field. In the pulsed OPA experiments reported to date [4–6,13] the LO pulse was somewhat longer than the squeezed signal pulse since it was derived from the fundamental beam before frequency doubling (in a wide-bandwidth crystal) to produce the pump pulse. The temporal mismatch between the squeezed light and the LO is one likely contributor to the degradation of the observed squeezing from values predicted by simple theories [13]. The other important factor is spatial behavior, discussed by LaPorta and Slusher [14].

The temporal mode matching of squeezed and LO pulses plays an important role in the generation and detection of squeezed pulses using temporally incoherent light [6]. Titulaer and Glauber [15] demonstrated that nonmonochromatic modes can be first-order coherent, allowing the possibility of a general time-dependent field as an excitation of a single spatiotemporal mode. However, the mode functions are not in general an orthonormal set. Kumar, Aytur, and Huang suggest that in order to optimally detect the squeezing generated, one needs the temporal profile of the local oscillator to be that of the squeezed mode [6]. While this choice might be optimal in a practical sense, we will show that it is not optimal for single short pulses.

In the steady-state pump case the effects of dispersion in the parametric medium have been theoretically treated by several authors [16–19]. It was found that the phase-matching bandwidth of the down-conversion process limits the bandwidth of the quadrature squeezing, as would be expected. In realistic crystals (of length 1 cm) this phase-matching bandwidth is typically of the order 3×10^{14} rad/sec.

A treatment combining the effects of finite pulse duration and dispersion was provided by Raymer, Drummond, and Carter [11]. They introduced the positive-P representation to calculate numerically the squeezing spectrum. The results presented were for a classical undepleted pump and a local oscillator taken to be the square root of the pump pulse. It was shown that the generated squeezing had a bandwidth that was limited by the group-velocity dispersion and for pump pulse widths less than the inverse phase-matching bandwidth would result in a significant reduction in detected squeezing. The present paper presents a more complete analysis of this model and explores its predictions for realistic experimental cases, including LO pulse shaping as a means for detecting larger squeezing.

II. EQUATIONS OF MOTION

The traveling-wave parametric amplifier is modeled here as a nonlinear, dispersive dielectric waveguide that allows propagation in the z direction in single transverse modes for both the fundamental (signal) and the second harmonic (pump) and is orientated such that type-I phase matching for the $\chi^{(2)}$ process is dominant. The Hamiltonian used here is the same as that appearing in the earlier work of Raymer *et al.* [11],

$$\hat{H} = \sum_m \hbar\omega_m^{(1)} \hat{a}_m^{(1)\dagger} \hat{a}_m^{(1)} + \sum_m \hbar\omega_m^{(2)} \hat{a}_m^{(2)\dagger} \hat{a}_m^{(2)} - \frac{1}{3}\epsilon_0 \chi^{(2)} \int d^3x : \left[\frac{\hat{D}^{(1)}(\mathbf{x})}{\epsilon_1} + \frac{\hat{D}^{(2)}(\mathbf{x})}{\epsilon_2} \right]^3 : \quad (1)$$

where the notation : : represents normal ordering. Here the electric displacements $D^{(i)}(\mathbf{x})$ in the nonlinear term are expanded in terms of the boson field operators as

$$\hat{D}^{(i)}(\mathbf{x}) = i \sum_m \left(\frac{\epsilon_i \hbar \omega_i' k_0^{(i)}}{2L} \right)^{1/2} \hat{a}_m^{(i)} u^{(i)}(\mathbf{x}) \exp\left(i k_m^{(i)} z \right) + \text{H.a.}, \quad (2)$$

where the frequency dependence of the parameters has been kept only for the phase-shift term $\exp(ik_m^{(i)} z)$. The electric permittivity at frequencies ω_1 and ω_2 are given by ϵ_1 and ϵ_2. The annihilation operators $\hat{a}_m^{(i)}$ correspond to a mode with propagation constant

$$k_m^{(i)} = \left(\frac{\epsilon_i}{\epsilon_0} \right)^{1/2} \frac{\omega_i}{c} + m\Delta k, m = -M, \ldots, M \quad (3)$$

with mode spacing $\Delta k = 2\pi/L$. The mode volume is then defined by the normalized transverse mode function $u^{(i)}(\mathbf{x})$ and the length L of the medium. Here $\mathbf{x}$ represents the transverse coordinates. The mode frequencies $\omega_m^{(i)}$ are approximate, corresponding to a second-order Taylor expansion, so that

$$\omega_m^{(i)} \approx \omega_i + (m\Delta k)\,\omega_i' + \frac{1}{2}(m\Delta k)^2 \omega_i'', \quad (4)$$

where the derivatives ω_i' and ω_i'' are with respect to k. This is easily extended to include higher-order dispersion if desired. The procedure for transforming to local field operators has been given in the work of Drummond and Carter [20]. The local field operators are defined on a lattice of length L with $2M+1$ points by

$$\hat{\alpha}_l = \frac{1}{\sqrt{2M+1}} \sum_{m=-M}^{M} \hat{a}_m^{(1)} \exp\left(\frac{i2\pi m l}{2M+1} \right) \quad (5)$$

so that the lattice cell denoted by l corresponds to the longitudinal position $z_l = l\Delta z = lL/(2M+1)$. Local operators $\hat{\beta}_l$ are defined analogously from the $\hat{a}_m^{(2)}$ operators. The Hamiltonian can be written in an interaction picture, which removes the carrier frequency oscillations, as

$$\hat{H}/\hbar = \sum_l \sum_{l'} \Delta\omega^{\alpha}_{ll'} \hat{\alpha}^{\dagger}_l \hat{\alpha}_{l'} + \sum_l \sum_{l'} \Delta\omega^{\beta}_{ll'} \hat{\beta}^{\dagger}_l \hat{\beta}_{l'} \tag{6}$$

$$+ \left[\frac{1}{2} i\chi^* \omega_1' \left(\frac{\omega_2'}{\Delta z} \right)^{1/2} \sum_l \hat{\alpha}_l^{\dagger^2} \hat{\beta}_l e^{-i(2k_0^{(1)} - k_0^{(2)})z_l} + \text{H.a.} \right], \tag{7}$$

where the definition of $\Delta\omega_{ll'}$ follows directly [20] from substituting Eq. (5) into Eq. (1) and

$$\chi = \frac{\epsilon_0 \chi^{(2)} k_0^{(1)}}{\epsilon_1} \left(\frac{\hbar k_0^{(2)}}{2\epsilon_2} \right)^{\frac{1}{2}} \int d^2\mathbf{x} \left[u^{(1)}(\mathbf{x}) \right]^2 u^{(2)^*}(\mathbf{x}). \tag{8}$$

It is instructive to use the s-parametrized quasiprobability distributions of Cahill and Glauber [21], which we denote by $W(\boldsymbol{\alpha}, \boldsymbol{\beta}; s, t)$. With these distribution functions, s-ordered products $\langle \{(a^{\dagger})^n a^m\}_s \rangle$ can be obtained by integration in the complex α plane according to

$$\langle \{(a^{\dagger})^n a^m\}_s \rangle = \int (\alpha^*)^n \alpha^m W(\alpha; s, t) d^2\alpha. \tag{9}$$

The parameter $s = 1, 0, -1$ corresponds to normal, symmetric, and antinormal ordered products and the P, Wigner, and Q quasiprobability distributions, respectively. The evolution equation for the s-parametrized quasiprobability densities is obtained from the Liouville equation for the density operator in the usual way [22] and is

$$\frac{\partial}{\partial t} W(\boldsymbol{\alpha}, \boldsymbol{\beta}; s, t) = \left[\sum_l -\frac{\partial}{\partial \alpha_l} \left(-i \sum_{l'} \Delta\omega^{\alpha}_{ll'} \alpha_{l'} + \chi_l^* \alpha_l^* \beta_l \right) + \sum_l -\frac{\partial}{\partial \alpha_l^*} \left(+i \sum_{l'} \Delta\omega^{\alpha}_{l'l} \alpha_{l'}^* + \chi_l \alpha_l \beta_l^* \right) \right.$$
$$+ \sum_l -\frac{\partial}{\partial \beta_l} \left(-i \sum_{l'} \Delta\omega^{\beta}_{ll'} \beta_{l'} - \frac{1}{2} \chi_l \alpha_l^2 \right) + \sum_l -\frac{\partial}{\partial \beta_l^*} \left(+i \sum_{l'} \Delta\omega^{\beta}_{l'l} \beta_{l'}^* - \frac{1}{2} \chi_l^* \alpha_l^{*2} \right)$$
$$+ \sum_l s \frac{\chi_l^*}{2} \frac{\partial^2}{\partial \alpha_l^2} \beta_l + \sum_l s \frac{\chi_l}{2} \frac{\partial^2}{\partial \alpha_l^{*2}} \beta_l^*$$
$$\left. + \frac{\chi_l^*}{8} (1 - |s|) \sum_l \frac{\partial^3}{\partial \alpha_l^2 \partial \beta_l^*} + \frac{\chi_l}{8} (1 - |s|) \sum_l \frac{\partial^3}{\partial \alpha_l^{*2} \partial \beta_l} \right] W(\boldsymbol{\alpha}, \boldsymbol{\beta}; s, t), \tag{10}$$

where $\chi_l = \omega_1' \sqrt{\omega_2'/\Delta z} \chi \exp[i(2k_0^{(1)} - k_0^{(2)})z_l]$. The evolution equation for $W(\boldsymbol{\alpha}, \boldsymbol{\beta}; s, t)$ corresponds to a multivariate Fokker-Planck equation for the P and the Q representations. By rewriting the differential operators and amplitudes in scaled variables, we can see the contribution given by each component. The scaling is related to the peak photon flux of the pump so that the evolution equation becomes

$$\frac{\partial}{\partial t} W(\boldsymbol{\alpha}, \boldsymbol{\beta}; s, t) = \left[\sum_l -\frac{\partial}{\partial \bar{\alpha}_l} \left(-i \sum_{l'} \Delta\omega^{\alpha}_{ll'} \bar{\alpha}_{l'} + \frac{\chi_l^*}{\epsilon} \bar{\alpha}_l^* \bar{\beta}_l \right) + \sum_l -\frac{\partial}{\partial \bar{\alpha}_l^*} \left(+i \sum_{l'} \Delta\omega^{\alpha}_{l'l} \bar{\alpha}_{l'}^* + \frac{\chi_l}{\epsilon} \bar{\alpha}_l \bar{\beta}_l^* \right) \right.$$
$$+ \sum_l -\frac{\partial}{\partial \bar{\beta}_l} \left(-i \sum_{l'} \Delta\omega^{\beta}_{ll'} \bar{\beta}_{l'} - \frac{1}{2\epsilon} \chi_l \bar{\alpha}_l^2 \right) + \sum_l -\frac{\partial}{\partial \bar{\beta}_l^*} \left(+i \sum_{l'} \Delta\omega^{\beta}_{l'l} \bar{\beta}_{l'}^* - \frac{1}{2\epsilon} \chi_l^* \bar{\alpha}_l^{*2} \right)$$
$$+ \sum_l s \frac{\epsilon \chi_l^*}{2} \frac{\partial^2}{\partial \bar{\alpha}_l^2} \bar{\beta}_l + \sum_l s \frac{\epsilon \chi_l}{2} \frac{\partial^2}{\partial \bar{\alpha}_l^{*2}} \bar{\beta}_l^*$$
$$\left. + \frac{\epsilon^3 \chi_l^*}{8} (1 - |s|) \sum_l \frac{\partial^3}{\partial \bar{\alpha}_l^2 \partial \bar{\beta}_l^*} + \frac{\epsilon^3 \chi_l}{8} (1 - |s|) \sum_l \frac{\partial^3}{\partial \bar{\alpha}_l^{*2} \partial \bar{\beta}_l} \right] W(\boldsymbol{\alpha}, \boldsymbol{\beta}; s, t), \tag{11}$$

where $\bar{\alpha}_l = \epsilon \alpha_l$ and $\bar{\beta}_l = \epsilon \beta_l$ so the system size parameter $\epsilon = \bar{n}^{-1/2}$ allows the third-order derivatives to be dropped for large $\bar{n}$. An explicit expression for $\bar{n}$ will appear later once we scale the evolution equations for $\boldsymbol{\alpha}, \boldsymbol{\beta}$. The two distributions of interest here are the Wigner and the positive-P distributions. We can extract the Wigner results directly from above with $s = 0$. For the positive-P representation [23], we need to double the phase-space dimension of the usual P representation whose evolution equation is given above with $s = 1$. Now we consider the parameter s to be restricted to $\{0, 1\}$, where $s = 1$ now corresponds to the positive-P representation. Dropping the third-order derivatives for $s = 0$ in Eq. (10), the corresponding Ito stochastic differential equations are

$$\frac{\partial \alpha_l}{\partial t} = -i \sum_{l'} \Delta\omega^{\alpha}_{ll'} \alpha_{l'} + \chi_l^* \alpha_l^{\dagger} \beta_l + s \sqrt{\chi_l^* \beta_l} \zeta_l(t),$$
$$\frac{\partial \alpha_l^{\dagger}}{\partial t} = +i \sum_{l'} \Delta\omega^{\alpha}_{l'l} \alpha_{l'}^{\dagger} + \chi_l \alpha_l \beta_l^{\dagger} + s \sqrt{\chi_l \beta_l^{\dagger}} \zeta_l^{\dagger}(t),$$
$$\frac{\partial \beta_l}{\partial t} = -i \sum_{l'} \Delta\omega^{\beta}_{ll'} \beta_{l'} - \frac{1}{2} \chi_l \alpha_l^2,$$
$$\frac{\partial \beta_l^{\dagger}}{\partial t} = +i \sum_{l'} \Delta\omega^{\beta}_{l'l} \beta_{l'}^{\dagger} - \frac{1}{2} \chi_l^* \alpha_l^{\dagger^2}, \tag{12}$$

where the noises are real Gaussian stochastic processes with correlations given by

$$\langle \zeta_l(t)\zeta_{l'}(t')\rangle = \delta_{ll'}\delta(t-t'),$$

$$\langle \zeta_l(t)\zeta_{l'}^{\dagger}(t')\rangle = \langle \zeta_l(t)\rangle = \langle \zeta_l^{\dagger}(t)\rangle = 0.$$

It is important to note that in the positive-P representation $\alpha_l^{\dagger}$ ($\beta_l^{\dagger}$) is not necessarily the complex conjugate of α_l (β_l), except in the mean. The derivation of the evolution equation for $W(\boldsymbol{\alpha},\boldsymbol{\beta};s,t)$ relies upon the use of partial integration and assumes that the distribution is sufficiently rapidly vanishing at the phase-space boundaries where $|\alpha_l|,|\beta_l| \to \infty$. The equivalence between a Fokker-Planck equation with second-order derivatives and stochastic differential equations also requires a positive semidefinite diffusion, which Eq. (10) does not provide explicitly. However, an evolution equation for the positive-P distribution ($s=1$) can always be found such that it has a positive semidefinite diffusion using the nonuniqueness of the time development of $W(\boldsymbol{\alpha},\boldsymbol{\beta})$ corresponding to the original master equation [23]. Given that such a diffusion matrix exists and it is the noise correlations of the SDE's that are the important property, one can write down a convenient noise term with the appropriate correlations. There are no third-order derivative terms in the case of the positive-P representation, so no additional assumptions are needed to transform the Fokker-Planck equation into stochastic equations.

In the Wigner case (with $s=0$), the equations of motion are classical and all the quantum noise enters in the initial conditions. However, the final truncated or "semiclassical" equation is only approximate since it requires the neglect of third-order derivative terms. This approximation is justified by the argument that, with large photon numbers, ϵ is relatively small. The large photon-number approximation is difficult to check directly and can lead to incorrect results if higher-order correlations are calculated. However, we can compare results with the $s=1$ case, since the neglect of boundary terms in the positive-P simulations is readily justified for the parameters used here, from the numerical results (which show no signs of large excursions). A comparison of these results with our Wigner simulations demonstrates agreement for squeezing calculations with our choice of parameters and interaction lengths.

Either type of equation can be transformed to evolve photon flux amplitudes by defining

$$\Phi_l = \alpha_l\left(\frac{\omega_1'}{\Delta z}\right)^{1/2},$$

$$\Psi_l = \beta_l\left(\frac{\omega_2'}{\Delta z}\right)^{1/2}, \tag{13}$$

where $\Phi_l^{\dagger}\Phi_l$ and $\Psi_l^{\dagger}\Psi_l$ equal the number of photons per second passing the z_l plane for signal and pump fields, respectively. This gives

$$\frac{\partial\Phi_l}{\partial t} = -i\sum_{l'}\Delta\omega_{ll'}^{\alpha}\Phi_{l'} + \chi_l^{*}\Phi_l^{\dagger}\Psi_l\left(\frac{\Delta z}{\omega_2'}\right)^{1/2} + s\sqrt{\omega_1'\chi_l^{*}\left(\frac{\Delta z}{\omega_2'}\right)^{1/2}\Psi_l}\frac{\zeta_l(t)}{\sqrt{\Delta z}},$$

$$\frac{\partial\Phi_l^{\dagger}}{\partial t} = +i\sum_{l'}\Delta\omega_{l'l}^{\alpha}\Phi_{l'}^{\dagger} + \chi_l\Phi_l\Psi_l^{\dagger}\left(\frac{\Delta z}{\omega_2'}\right)^{1/2} + s\sqrt{\omega_1'\chi_l\left(\frac{\Delta z}{\omega_2'}\right)^{1/2}\Psi_l^{\dagger}}\frac{\zeta_l^{\dagger}(t)}{\sqrt{\Delta z}},$$

$$\frac{\partial\Psi_l}{\partial t} = -i\sum_{l'}\Delta\omega_{ll'}^{\beta}\Psi_{l'} - \frac{1}{2}\chi_l\Phi_l^2\frac{\sqrt{\Delta z\omega_2'}}{\omega_1'},$$

$$\frac{\partial\Psi_l^{\dagger}}{\partial t} = +i\sum_{l'}\Delta\omega_{l'l}^{\beta}\Psi_{l'}^{\dagger} - \frac{1}{2}\chi_l^{*}\Phi_l^{\dagger^2}\frac{\sqrt{\Delta z\omega_2'}}{\omega_1'}. \tag{14}$$

We now transform to a comoving frame at speed ω_1' and evaluate the terms involving $\Delta\omega_{ll'}$ that are related to the discretized first and second derivatives with respect to z. We retain only the first-order derivative in z in the comoving frame to give continuum equations for $\Phi(z,t_v)$ and $\Psi(z,t_v)$:

$$\left(\frac{\partial}{\partial z} + \frac{i}{2}k_1''\frac{\partial^2}{\partial {t_v}^2}\right)\Phi = \chi^{*}\Phi^{\dagger}\Psi + s\sqrt{\chi^{*}\Psi}\zeta(z,t_v), \tag{15a}$$

$$\left(\frac{\partial}{\partial z} - \frac{i}{2}k_1''\frac{\partial^2}{\partial {t_v}^2}\right)\Phi^{\dagger} = \chi\Psi^{\dagger}\Phi + s\sqrt{\chi\Psi^{\dagger}}\zeta^{\dagger}(z,t_v), \tag{15b}$$

$$\left[\frac{\partial}{\partial z} + \left(\frac{1}{\omega_2'} - \frac{1}{\omega_1'}\right)\frac{\partial}{\partial t_v} - i\left(k_0^{(2)} - 2k_0^{(1)}\right) + \frac{i}{2}k_2''\frac{\partial^2}{\partial {t_v}^2}\right]\Psi = -\frac{1}{2}\chi\Phi^2, \tag{15c}$$

$$\left[\frac{\partial}{\partial z} + \left(\frac{1}{\omega_2'} - \frac{1}{\omega_1'}\right)\frac{\partial}{\partial t_v} + i\left(k_0^{(2)} - 2k_0^{(1)}\right) - \frac{i}{2}k_2''\frac{\partial^2}{\partial {t_v}^2}\right]\Psi^{\dagger} = -\frac{1}{2}\chi^{*}\Phi^{\dagger^2}, \tag{15d}$$

where $t_v = t - z/v, k_i'' = d^2k/d\omega^2|_{k=k_i} = -\omega_i''/v^3$, and t is the time measured in the laboratory frame while t_v is the time measured in the comoving frame with speed $v=\omega_1'$. The factor $(k_0^{(2)} - 2k_0^{(1)})$ accounts for any mismatch of phase velocities, while $(1/\omega_2' - 1/\omega_1')$ accounts for group-velocity mismatch and k_i'' accounts for group-velocity dispersion (GVD). These equations can be cast into the dimensionless equations

$$\frac{\partial\phi}{\partial\xi} = -\frac{i}{2}\mathrm{sgn}(k_1'')\frac{\partial^2}{\partial\tau^2}\phi + \phi^{\dagger}\psi + s\sqrt{\psi}\zeta(\xi,\tau), \tag{16a}$$

$$\frac{\partial\phi^{\dagger}}{\partial\xi} = +\frac{i}{2}\mathrm{sgn}(k_1'')\frac{\partial^2}{\partial\tau^2}\phi^{\dagger} + \phi\psi^{\dagger} + s\sqrt{\psi^{\dagger}}\zeta^{\dagger}(\xi,\tau), \tag{16b}$$

$$\frac{\partial\psi}{\partial\xi} = \left[\frac{z_0}{t_0}\left(\frac{1}{\omega_1'} - \frac{1}{\omega_2'}\right)\frac{\partial}{\partial\tau} + iz_0\left(k_0^{(2)} - 2k_0^{(1)}\right) - \frac{i}{2}\frac{k_2''}{|k_1''|}\left(\frac{\omega_2'}{\omega_1'}\right)^2\frac{\partial^2}{\partial\tau^2}\right]\psi - \frac{1}{2}\phi^2, \tag{16c}$$

$$\frac{\partial\psi^\dagger}{\partial\xi} = \left[\frac{z_0}{t_0}\left(\frac{1}{\omega_1'} - \frac{1}{\omega_2'}\right)\frac{\partial}{\partial\tau} - iz_0\left(k_0^{(2)} - 2k_0^{(1)}\right) + \frac{i}{2}\frac{k_2''}{|k_1''|}\left(\frac{\omega_2'}{\omega_1'}\right)^2\frac{\partial^2}{\partial\tau^2}\right]\psi^\dagger - \frac{1}{2}\phi^{\dagger 2}, \tag{16d}$$

where $\xi = z/z_0$ is the propagation distance scaled by z_0 and $\tau = t_v/t_0$ is the scaled time in the comoving frame. Here $z_0 = |\chi\Psi_0|^{-1}$ is the classical undepleted pump gain length and $t_0 = \sqrt{z_0 k_1''}$ is the inverse phase-matching bandwidth when Ψ_0 is the initial peak value of Ψ. The noise correlation is

$$\langle\zeta(\xi,\tau)\zeta(\xi',\tau')\rangle = \frac{1}{\bar{n}}\delta(\xi-\xi')\delta(\tau-\tau'), \tag{17}$$

where $\bar{n} = \Psi_0^2 t_0$ is the parameter governing the system size expansion. The dimensionless fields ϕ and ψ are defined by $\phi = \Phi/\Psi_0$ and $\psi = \Psi/\Psi_0$.

In the Wigner representation the evolution of the field $\phi(\xi,\tau)$ is governed by Eq. (16) with $s = 0$ provided the parameter governing the system size expansion $\epsilon = \bar{n}^{-1/2}$ is sufficiently small that the third-order derivatives in the evolution equation for the Wigner function can be neglected. This means that the photon number of the quantized pump pulse has to be sufficiently large and the propagation distances sufficiently short ($\xi \ll \bar{n}^{1/2}$). This is in contrast to the positive-P representation for which Eq. (16) is exact (in the absence of boundary terms), since the Hamiltonian is only quadratic in boson creation operators for the subharmonic field and linear for the pump field. If, however, the Hamiltonian does not include a quantized pump, then the partial differential equations with $s = 0$ correspond exactly to the Fokker-Planck equation for W and give identical results to the positive-P representation. We note that for the parametric amplifier there are no additional self-frequency shifts introduced by using the Wigner representation, as in the case of the quantum nonlinear Schrödinger equation [24]. In the Wigner representation the dynamics is restricted to the classical subspace $\{\phi^\dagger,\psi^\dagger\} = \{\phi^*,\psi^*\}$ so that the boundary conditions at $\xi = 0$ for an input coherent state can be written (neglecting the nonzero mean amplitude) as $\phi(0,\tau) = \Delta\phi(0,\tau)$ and $\psi(0,\tau) = \Delta\psi(0,\tau)$ and

$$\langle\Delta\phi(0,\tau)\Delta\phi^*(0,\tau')\rangle = \frac{1}{2\bar{n}}\delta(\tau-\tau'),$$
$$\langle\Delta\psi(0,\tau)\Delta\psi^*(0,\tau')\rangle = \frac{1}{2\bar{n}}\left(\frac{\omega_2'}{\omega_1'}\right)\delta(\tau-\tau'), \tag{18}$$

where $\Delta\phi$ and $\Delta\psi$ represent delta-correlated Gaussian stochastic processes with a mean of zero. Because $s = 0$ in this representation, the distributed noise $\zeta(\xi,\tau)$ does not contribute in Eq. (16).

III. ANALYTIC SOLUTIONS IN LIMITING CASES

In this section we solve Eqs. (16) in several special cases, as a guide to some of the qualitative physical properties of the full dynamics, which are studied numerically and presented in Secs. IV and V.

A. cw pump with dispersion

Here we use the positive-P representation to solve directly for the $\tilde{\phi}(\xi,\omega)$ field used in calculating the squeezing spectrum. In the positive-P representation, the subharmonic field evolution for a constant pump is of similar form to the linearized nonlinear Schrödinger equation discussed by Drummond and Carter [20]. For an initial vacuum state for $\phi(0,\tau)$ and a constant pump in a coherent state $\psi(\xi,\tau) = i/2$, the evolution of the subharmonic field as given by Eqs. (16a) and (16b) is given by

$$\frac{\partial\phi}{\partial\xi} = \frac{i}{2}\left[-\mathrm{sgn}(k_1'')\frac{\partial^2}{\partial\tau^2}\phi + \phi^\dagger\right] + \sqrt{\frac{i}{2}}\zeta(\xi,\tau), \tag{19}$$

$$\frac{\partial\phi^\dagger}{\partial\xi} = \frac{i}{2}\left[\mathrm{sgn}(k_1'')\frac{\partial^2}{\partial\tau^2}\phi^\dagger - \phi\right] + \sqrt{\frac{i}{2}}i\zeta^\dagger(\xi,\tau). \tag{20}$$

These two coupled equations can be integrated directly in Fourier space to give

$$\tilde{\phi}(\xi,\omega) = \left(\frac{i}{2}\right)^{1/2}\int_0^\xi d\xi'\left\{\cos[\gamma(\xi-\xi')/2] + i\frac{\beta}{\gamma}\sin[\gamma(\xi-\xi')/2]\right\}\zeta(\xi,\omega) - \left(\frac{i}{2}\right)^{1/2}\int_0^\xi d\xi'\frac{1}{\gamma}\sin[\gamma(\xi-\xi')/2]\times\zeta^\dagger(\xi,\omega), \tag{21}$$

where $\gamma = (\omega^4-1)^{1/2}$, $\beta = \pm\omega^2$, and

$$\tilde{\phi}(\xi,\omega) = \frac{1}{\sqrt{2\pi}}\int d\tau e^{i\omega\tau}\phi(\xi,\tau). \tag{22}$$

Equivalent solutions for this case have been given previously [17–19]. The normalized maximum squeezing spectrum is defined as

$$S_{\max}(\xi,\omega) = 2\bar{n}[\langle\tilde{\phi}(\xi,-\omega)\tilde{\phi}^\dagger(\xi,\omega)\rangle - |\langle\tilde{\phi}(\xi,-\omega)\tilde{\phi}(\xi,\omega)\rangle|] \tag{23}$$

and corresponds to the optimum and independent choice of LO phase at each frequency. This represents the noise seen in a quadrature-field measurement using a balanced homodyne detector, consisting of a beam splitter to equally mix the signal with the LO, and two photodiodes whose currents are subtracted and spectrally analyzed. We find

$$S_{\max}(\xi,\omega)=\frac{[1-\cos(\gamma\xi)]}{\gamma^2}-\left|i\frac{\sin(\gamma\xi)}{\gamma}+\frac{\beta}{\gamma^2}[1-\cos(\gamma\xi)]\right| \quad (24)$$

so that the maximum dc squeezing is simply

$$S_{\max}(\xi,0)=-1+e^{-\xi}. \quad (25)$$

The shot-noise level is defined by $S(\xi,\omega)=0$ and $S(\xi,\omega)=-1$ is perfect squeezing. Since the pump is constant in this case, treating the pump as a c number is the same as a coherent state in a P representation so that the Wigner representation (with a c-number pump field) is exact and hence must give identical results.

Comparing this result to that given by Drummond and Carter [20] for the linearized nonlinear Schrödinger equation given by

$$\frac{\partial\delta\phi}{\partial\xi}=-\frac{i}{2}\left[\mathrm{sgn}(k'')\frac{\partial^2}{\partial\tau^2}-1\right]\delta\phi+\frac{i}{2}\delta\phi^{\dagger}+\sqrt{\frac{i}{2}}\zeta(\xi,\tau), \quad (26)$$

where $\phi=1/\sqrt{2}+\delta\phi$ and the maximum squeezing spectrum is

$$S_{\max}(\xi,\omega)=\frac{[1-\cos(\gamma\xi)]}{\gamma^2}-\left|i\frac{\sin(\gamma\xi)}{\gamma}+\frac{\beta}{\gamma^2}[\cos(\gamma\xi)-1]\right|, \quad (27)$$

where $\gamma=\omega(\omega^2\pm2)^{1/2}$ and $\beta=(1\pm\omega^2)$. Despite the similarity between the evolution equations there is an important difference in the squeezing spectrum. The squeezing spectrum for the linearized nonlinear Schrödinger equation is very different for anomalous and normal dispersion regimes whereas the parametric amplifier shows no such distinction when phase matched.

B. Pulsed pump with no dispersion

With no dispersion each quadrature is independent and the phase-matching bandwidth is infinite, allowing the $\phi(\xi,t_v)$ field to be integrated directly, giving the usual exponential dependence. In this case there is no need to solve coupled equations and so the Wigner representation is employed. In the Wigner representation, the subharmonic field evolution for nondispersive propagation with classical undepleted pulsed pump and equal group velocities is given by [12,25]

$$\phi(\xi,t_v)=\phi(0,t_v)\cosh[|\psi(t_v)|\xi]+e^{i2\theta}\phi^*(0,t_v)\sinh[|\psi(t_v)|\xi], \quad (28)$$

where θ is the phase difference between ψ and χ. The normalized maximum squeezing [12] is equal at all frequencies and is given by

$$S_{\max}(\xi,\omega)=\frac{\int_{-T/2}^{T/2}dt\,\phi_{\mathrm{LO}}^2(t)\left(e^{-2|\psi(t)|\xi}-1\right)}{\int_{-T/2}^{T/2}dt\,\phi_{\mathrm{LO}}^2(t)}, \quad (29)$$

where the measurement period T corresponds to the detection integration time in laboratory time units. Using a local oscillator amplitude $\phi_{\mathrm{LO}}(t)=\mathrm{sech}(t/t_{\mathrm{LO}})$ with pulse width t_{LO} measured in the same units as T and pump amplitude $\psi(t)=\mathrm{sech}^2(t_v/t_P)$ with pulse width t_P, the maximum dc-squeezing as predicted by Eq. (29) is shown in Fig. 1 and predicts maximum squeezing for $t_{\mathrm{LO}}\ll t_P$. There is also a finite amount of squeezing for long local oscillator pulses ($t_{\mathrm{LO}}>t_P$), which is determined by the integral

$$S_{\max}(\xi,\omega)=\frac{\int_{-T/2}^{T/2}dt\,\left\{\exp\left[-2\mathrm{sech}^2(t/t_P)\xi\right]-1\right\}}{2\tanh(T/2)}. \quad (30)$$

Consider the result for equal pulse widths $t_{\mathrm{equal}}=t_{\mathrm{LO}}=t_P$ for the local oscillator and pump, where now $\psi(t)=\frac{1}{2}\mathrm{sech}^2(t_v/t_P)$ so that the peak amplitude corresponds to that used earlier for the cw result. In this case the result can be found to be

$$S_{\max}(\xi,\omega)=-1-\frac{i}{2}\sqrt{\frac{\pi}{\xi}}e^{-\xi}\coth\left(\frac{T}{2t_{\mathrm{equal}}}\right)\times\mathrm{erf}\left[i\sqrt{\xi}\tanh\left(\frac{T}{2t_{\mathrm{equal}}}\right)\right], \quad (31)$$

which in the limit of long pulse widths gives

$$\lim_{t_{\mathrm{equal}}\to\infty}S_{\max}(\xi,\omega)=-1+e^{-\xi}. \quad (32)$$

In this case, the nondispersive theory predicts the same squeezing for all frequencies and corresponds to the cw dispersive theory predictions for zero-frequency squeezing.

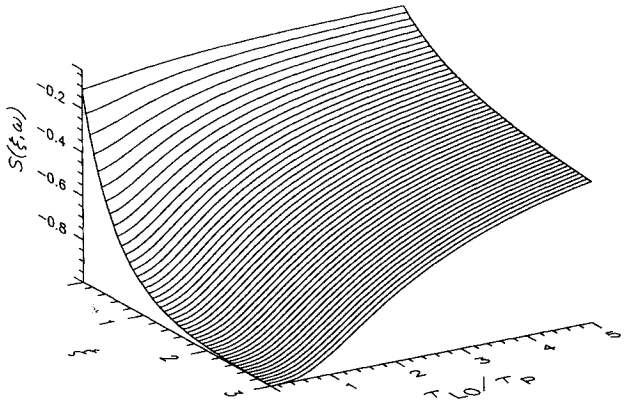

FIG. 1. Plot of squeezing with no dispersion versus propagation distance and the ratio of the local oscillator to pump pulse temporal widths.

IV. PULSED PUMP WITH SIGNAL DISPERSION

We now consider the dc squeezing for various local oscillator pulse widths while including signal dispersion and thus finite phase-matching bandwidth. The evolution considered is for a phase-matched interaction in a waveguide with no pump dispersion and equal group velocities for the subharmonic and pump pulses. This corresponds to Eqs. (16) with $k_2'' = 0, k_0^{(2)} = 2k_0^{(1)}$, and $\omega_2' = \omega_1'$. Pump depletion is included in all calculations for completeness. The system is idealized; however, it does allow one to investigate clearly the effects of the local oscillator pulse width on the detected noise reduction. We will later compare this result with the case of nonzero pump dispersion. We treat ideal, pulsed, balanced, homodyne detection and the quantity needed for calculating the squeezing spectrum is given by the normally ordered and time ordered operator expression [26,27]

$$2\pi\bar{n}^2\langle :\hat{X}(-\omega)\hat{X}(\omega):\rangle, \tag{33}$$

where

$$\hat{X}(\tau) = \hat{\phi}^\dagger(\tau)\hat{\phi}_{\rm LO}(\tau)e^{i\theta} + e^{-i\theta}\hat{\phi}_{\rm LO}^\dagger(\tau)\hat{\phi}(\tau), \tag{34}$$

where θ is an experimentally adjustable phase shift, $\hat{\phi}_{\rm LO}(\tau)$ is the pulsed local oscillator field operator, and $\hat{\phi}(\tau)$ is the signal field operator. One can calculate correlation functions such as Eq. (33) directly using the positive-P representation as ensemble averages correspond to normally ordered and time ordered moments. It is convenient to calculate a normalized squeezing spectrum such that the minimum value of the correlation function is -1, as in Sec. III. In the positive-P representation

$$\langle X(-\omega)X(\omega)\rangle \geq -\frac{1}{2\pi\bar{n}}\left\langle \int d\tau \left(\phi_{\rm LO}^\dagger\phi_{\rm LO} + \phi^\dagger\phi\right)\right\rangle, \tag{35}$$

where the angular brackets correspond to a stochastic average. Now we can define the pulsed squeezing spectrum as

$$S_\theta(\xi,\omega) = \frac{2\pi\bar{n}\langle :\hat{X}(\xi,-\omega)\hat{X}(\xi,\omega):\rangle}{\left\langle \int d\tau \left(\hat{\phi}_{\rm LO}^\dagger\hat{\phi}_{\rm LO} + \hat{\phi}^\dagger\hat{\phi}\right)\right\rangle}. \tag{36}$$

In the positive-P representation, the squeezing spectrum is then given by

$$S_\theta(\xi,\omega) = \frac{2\pi\bar{n}\langle X(\xi,-\omega)X(\xi,\omega)\rangle}{\left\langle \int d\tau \left(\phi_{\rm LO}^\dagger\phi_{\rm LO} + \phi^\dagger\phi\right)\right\rangle}. \tag{37}$$

In the Wigner representation, the stochastic moments correspond to symmetrical operator ordering resulting in the stochastic moment $\langle X(-\omega)X(\omega)\rangle$ being nonnegative. The squeezing spectrum in the Wigner representation is then

$$S_\theta(\xi,\omega) = -1 + \frac{2\pi\bar{n}\langle X(\xi,-\omega)X(\xi,\omega)\rangle}{\left\langle \int d\tau \left[|\phi_{\rm LO}|^2 + |\phi|^2 - 1/(\bar{n}\Delta\tau)\right]\right\rangle}, \tag{38}$$

where $\Delta\tau^{-1}$ is the frequency cutoff. The dc squeezing and dc unsqueezing $[1 + S_\theta(\xi,0)]$ using the positive-P and the truncated Wigner representations for no pump depletion or dispersion are compared in Fig. 2. The parameters were chosen such that the positive-P result corresponds to the earlier calculation presented in Ref. [11]. The results show agreement between the positive-P and the truncated Wigner representations. We note that the sampling error for the positive-P stochastic equations is more difficult to reduce in this system than for the squeezed solitons of the quantum nonlinear Schrödinger equation.

The dc squeezing calculated using the truncated Wigner representation, for a pulsed coherent state pump $\langle\psi(0,\tau)\rangle = \mathrm{sech}^2(\tau/\tau_P)$ with width $\tau_P = 5.0$ (in phase-matching bandwidth units t_0) and no pump dispersion, using a local oscillator pulse $\langle\phi_{\rm LO}(\tau)\rangle = \mathrm{sech}(\tau/\tau_{\rm LO})$ for various local oscillator pulse widths ranging from $\tau_{\rm LO} = 1.0, \ldots, 10.0$ is shown in Fig. 3. Perfect phase matching ($\Delta k = k_0^{(2)} - 2k_0^{(1)} = 0$) is assumed.

Several important points can be seen from the results in Fig. 3. Contrary to the prediction of Eq. (29), a shorter LO pulse is not necessarily better. The optimum local oscillator width in Fig. 3 lies between the inverse phase-matched bandwidth (1 in these units) and the pump

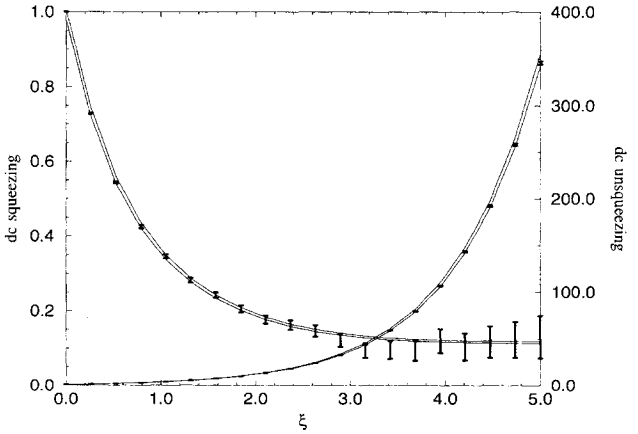

FIG. 2. Plot of dc squeezing and dc unsqueezing versus propagation distance with no pump depletion or dispersion using the positive-P and the truncated Wigner representations. Solid lines represent upper and lower limits of truncated Wigner results with 5000 trajectories. Error bars represent sampling errors using 100 000 positive-P trajectories with parameter values $\langle\psi(0,\tau)\rangle = \mathrm{sech}^2(\tau), \langle\phi_{\rm LO}(0,\tau)\rangle = \mathrm{sech}(\tau), k_0^{(2)} = 2k_0^{(1)}$, and $k_2'' = 0, \bar{n} = 10^9$.

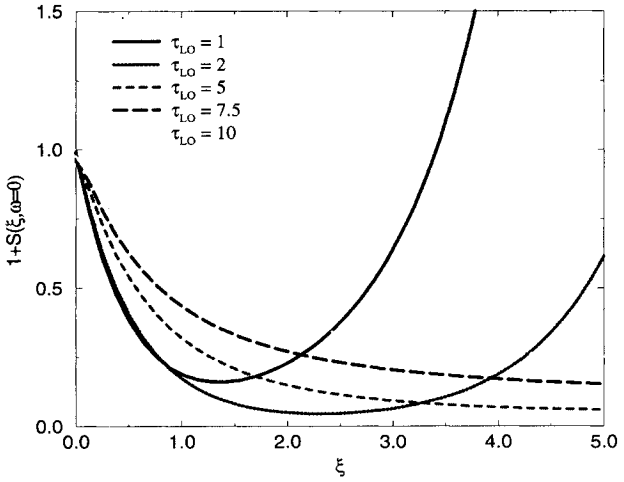

FIG. 3. Plot of dc squeezing versus propagation distance with no pump dispersion for various values of the local oscillator pulse width $\tau_{\rm LO} = 1, 2, 5, 7.5, 10$ corresponding to $\tau_{\rm LO}/\tau_P = 0.2, 0.4, 1.0, 1.5, 2.0$. The statistical errors are of the same order as the thickness of the lines in the regions of maximum squeezing (minimum S) and increase in either direction but remain less than ± 0.02. This is a Wigner simulation using 10 000 trajectories and parameter values $\langle\psi(0,\tau)\rangle = \mathrm{sech}^2(\tau/5)$, $\langle\phi_{\rm LO}(0,\tau)\rangle = \mathrm{sech}(\tau/\tau_{\rm LO})$, $k_0^{(2)} = 2k_0^{(1)}$, and $k_2'' = 0, \bar{n} = 10^{12}$.

width. This result is also in contrast to an assumption by Blow, Loudon, Pheonix, and Shepherd [28] that it is a generic property independent of the generation process that the local oscillator and signal pulses should have the same shape for optimum squeezing detection. If the local oscillator width is too short then it includes contributions from non-phase-matched frequencies. If the local oscillator is too long then the signal-LO overlap includes contributions from unsqueezed noise in the temporal wings of the subharmonic. That is, the squeezing generated by the pump pulse is localized in time and is of finite bandwidth due to the dispersion-limited phase-matching bandwidth.

It can also be seen from Fig. 3 that for each local oscillator pulse width there is an optimal propagation distance after which no improvement in the noise reduction is seen. As the signal propagates through the dispersive material, it develops a phase structure that eventually decreases the detected squeezing. Typically a device is used to alter the phase relationship between the local oscillator and the pump. This phase is optimized for each frequency component separately, which gives the maximum noise reduction for a particular realization of the local oscillator. Since dc squeezing detection involves averaging across the entire local oscillator and signal pulses, if the local oscillator has a different phase structure to the ensemble-averaged signal, then the detected field has contributions from different quadratures of the signal. An important effect to counteract is group-velocity dispersion induced frequency chirp. We show below that dispersing the local oscillator pulse by propagating through a medium with suitably chosen linear dispersion embeds approximately the correct type of phase structure to compensate the dispersive propagation of the signal through the nonlinear medium. Note that no pump dispersion was included for the results in Fig. 3 so that the pump pulse does not acquire a frequency chirp from group-velocity dispersion as it propagates. However, the squeezed vacuum does acquire a frequency chirp as it propagates.

In Fig. 4 we plot the dc squeezing for the same local oscillator pulse widths as in the previous figure, but include equal pump and signal dispersion (i.e., $k_2'' = k_1''$). All parameters except for the pump dispersion are the same as in Fig. 4. This shows that there is a negative effect on the detected noise reduction of the signal from the dispersing pump pulse. The dc squeezing for the shortest local oscillator pulse is, however, relatively unchanged by including the pump dispersion for the parameters we used here. One would expect that for shorter pump pulses the effect of pump dispersion would also be important for the shorter local oscillator pulse widths. One possibility that has not been explored here is that the negative effect of pump pulse dispersion can be reduced by pumping the parametric process at a frequency such that the pump and subharmonic experience group-velocity dispersion of opposite sign.

To illustrate the advantage of using a dispersed local oscillator, we compare the dc squeezing for nondispersed and dispersed local oscillators in Fig. 5. Using again $\tau_P = 5.0$, the nondispersed curve (dashed curve) corresponds to the result in Fig. 4 for $\tau_{\rm LO} = 2$ (and $k_{\rm LO}'' = 0$) while the full curve corresponds to exactly the same parameters except $k_{\rm LO}''/k_1'' = 0.2$. This means that the local oscillator pulse that is mixed at the beam splitter of the homodyne detector is treated as a seperate quan-

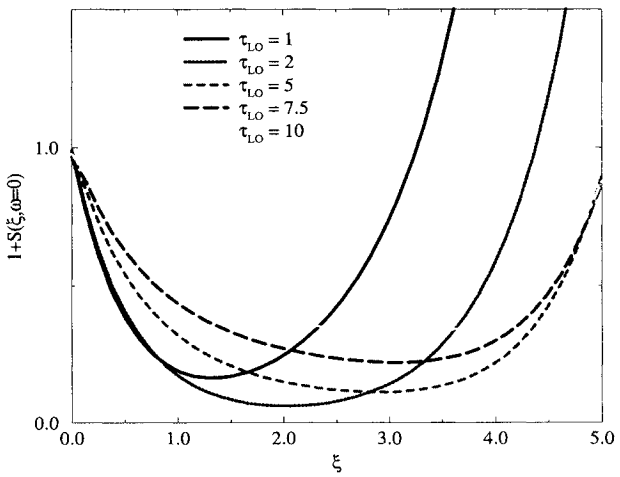

FIG. 4. Plot of dc squeezing versus propagation distance with pump and signal dispersion ($k_2'' = k_1''$). The statistical errors are within the same limits as in Fig. 3. This is a Wigner simulation using 10 000 trajectories and other parameter values are the same as in Fig. 3.

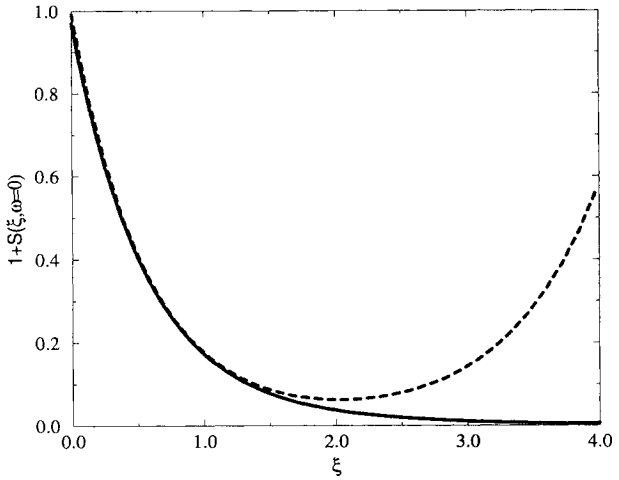

FIG. 5. Plot of dc squeezing versus propagation distance comparing dispersed (solid curve) and nondispersed (dashed curve) local oscillators. The initial LO duration is $\tau_{LO} = 2$ and other parameters are the same as in Fig. 4.

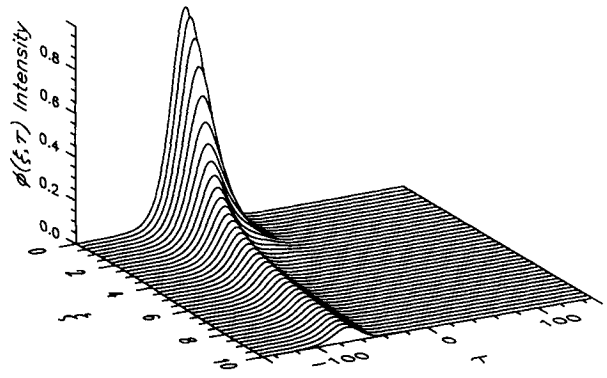

FIG. 6. Plot of pump intensity at 830 nm in LBO versus propagation distance including group-velocity mismatch and group-velocity dispersion. The parameter values are $\phi(0,\tau) = \mathrm{sech}(\tau/17), k_0^{(2)} = 2k_0^{(1)}, t_0(\omega_1' - \omega_2')/|k_1''|\omega_1'\omega_2' = 11.75$, and $k_2'' = 2.278k_1''$.

tum field having passed through a linear dielectric of the same length and GVD 1/5 of that experienced by the signal. By using the dispersed LO, the maximum detected squeezing improves from $S = -0.938 \pm 0.001$ to $S = -0.9949 \pm 0.0001$. The LO GVD is optimal at approximately 1/5 of the signal GVD (for the parameters used here) because the LO pulse is temporally shorter than the signal produced from vacuum. Note, however, that the LO does not have a larger bandwidth than the signal as the LO is initially transform limited. By using a linear medium with a well chosen group-velocity dispersion, the phase structure of the LO (predominantly the frequency chirp) more closely follows that of the signal. If higher-order linear dispersion were important for the signal as well, then it too should be considered in choosing the properties of the LO dispersive medium. Such effects could also be easily included in our treatment.

V. REALISTIC EXPERIMENTAL CASE

We will now present some results for a more realistic case where we simulate a realistic experiment using a 150-fs (intensity full width at half maximum) modelocked titanium sapphire laser operating at 830 nm. We include group-velocity mismatch and group-velocity dispersion for both fields in both the frequency doubling and down-conversion media (see Table I). The laser pulses are first frequency doubled in an LiB_3O_5 (LBO) crystal assumed to correspond to 10 gain lengths in a 5-mm crystal. The frequency doubling was also simulated using Eq. (16) and the pulse shape of the frequency-doubled pulse at the output face ($\xi = 10$) was used as input to the down-conversion simulation. The pulse shapes obtained are given in Figs. 6 and 7, showing the pump intensity at 830 nm and the second-harmonic intensity at 415 nm, respectively. Figure 7 clearly shows the effect of group-velocity mismatch in the LBO crystal. In LBO, the group-velocity mismatch compensated GVD ratio $k_2''\omega_2'^2/2|k_1''|\omega_1'^2$ was taken to be 1.091, while the scaled walkoff $t_0(\omega_1' - \omega_2')/|k_1''|\omega_1'\omega_2'$ was taken to be 11.75. These frequency-doubled pulses pump a 5-mm β-BaB_2O_4 (BBO) crystal that is phase matched at 830 nm and the down-converted light is directed towards a homodyne detection system using local oscillator pulses derived from the original 830-nm pulses. In BBO, the group-velocity mismatch compensated GVD ratio $k_2''\omega_2'^2/2|k_1''|\omega_1'^2$ was taken to be 1.27, while the scaled walkoff $t_0(\omega_1' - \omega_2')/|k_1''|\omega_1'\omega_2'$ was taken to be 29.26. The generated pump pulse is asymmetric and broadened compared to the local oscillator. The group-velocity mismatch in LBO causes the asymmetry in the generated second-harmonic (pump) pulse, which travels slower than the 830-nm pulse in LBO. The nonlinear interaction tends to broaden the generated second harmonic as it lags the 830-nm pulse.

The squeezing spectrum is shown in Fig. 8 and indicates significant squeezing even with group-velocity mis-

TABLE I. Material parameters for LBO and BBO.

	k_1' (s m^{-1})	k_2' (s m^{-1})	k_1'' (s^2 m^{-1})	k_2'' (s^2 m^{-1})
LiB_3O_5[a]	5.432×10^{-9}	5.5495×10^{-9}	5×10^{-26}	1.139×10^{-25}
β-BaB_2O_4[b]	5.613×10^{-9}	5.783×10^{-9}	6.74×10^{-26}	1.82×10^{-25}

[a]Values were calculated from the Sellmeier equations presented in Ref. [30].
[b]Values were calculated from the Sellmeier equations presented in Ref. [31].

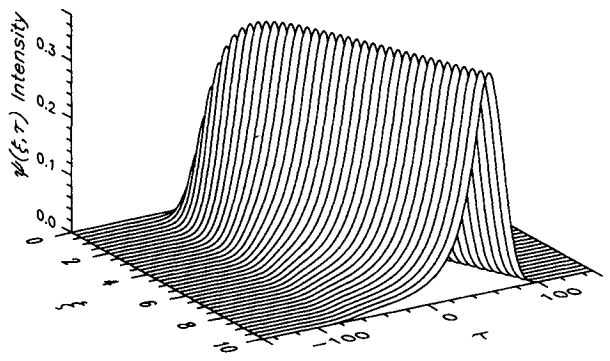

FIG. 7. Plot of second-harmonic intensity at 415 nm in LBO versus propagation distance including group-velocity mismatch and group-velocity dispersion. The parameter values are the same as in Fig. 6.

match and group-velocity dispersion. No local oscillator pulse shaping or dispersion was used in obtaining these results. Due to group-velocity mismatch in BBO, the local oscillator pulse has to be shifted with respect to the comoving frame in order to overlap with the generated squeezed pulse. This procedure has not been optimized, here but was allowed for in the simulations by giving the local oscillator a finite velocity. One expects that the asymmetry in the dynamical equations from a group-velocity mismatch will be reflected in the squeezing spectrum. As has been demonstrated, the group-velocity mismatch in LBO causes an asymmetric pump for the down-conversion in BBO. The scaled walkoff in BBO, which is larger than in LBO, results in the pump pulse lagging behind the signal field initially generated

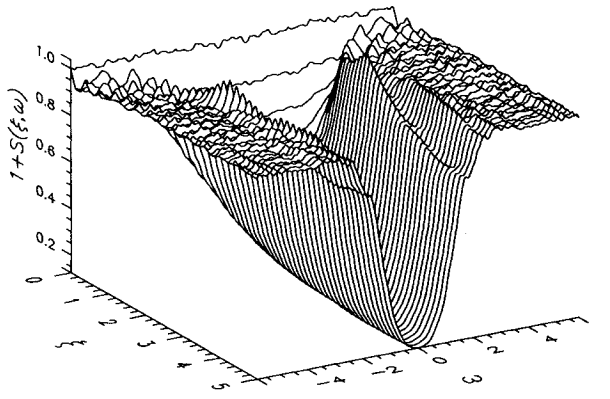

FIG. 8. Plot of squeezing spectrum versus propagation distance including group velocity mismatch and group-velocity dispersion. The local oscillator has been given a group-velocity such that it overlaps with the center of the signal at $\xi = 5$. This is a Wigner simulation using 10 000 trajectories with the parameter values $\langle\phi_{\rm LO}(0,\tau)\rangle = \mathrm{sech}(\tau/7.3), k_0^{(2)} = 2k_0^{(1)}, t_0(\omega_1' - \omega_2')/|k_1''|\omega_1'\omega_2' = 29.26$, and $k_2'' = 2.54k_1'', \bar{n} = 10^{12}$.

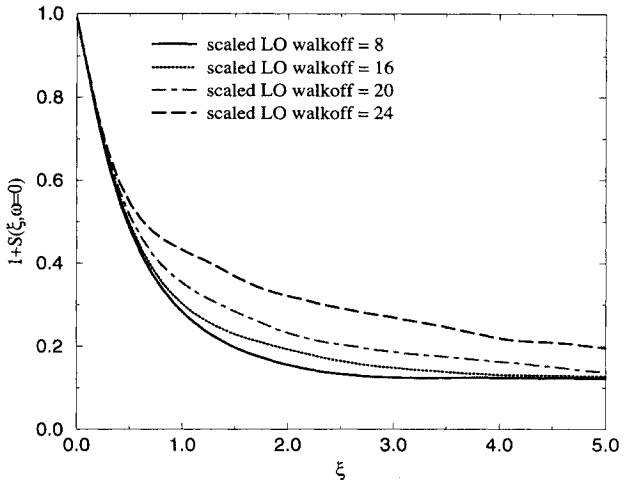

FIG. 9. Plot of dc squeezing versus propagation distance using the Wigner representation for various scaled local oscillator walkoffs equal to $t_0(\omega_1' - \omega_{\rm LO}')/|k_1''|\omega_1'\omega_{\rm LO}'$ and all other parameters are the same as in Fig. 8. A scaled local oscillator walkoff of 16 corresponds to the previous plot.

from vacuum. Typically, most of the squeezing is generated in the first one to two gain lengths. One would predict then that a local oscillator overlapping with the leading component of the signal pulse will detect more squeezing than one overlapping with the trailing component. This expectation is borne out by calculating the squeezing spectrum for various timings of the local oscillator. In an experiment, the timing of local oscillator pulse is adjusted by a delay line. Here this is simulated by varying the scaled walkoff of the local oscillator. The dc squeezing variations due to timing of local oscillator pulse are plotted in Fig. 9. This particular qualitative result has been verified in recent experiments using bulk crystals on which these parameters are based [9].

VI. CONCLUSION

We have presented a study of the pulsed, traveling-wave parametric amplifier, exploring the consequences of medium dispersion on the pump and signal fields, as well as amplitude and phase structure of the local oscillator pulses. Such dispersion strongly affects the level of detectable quadrature squeezing when the pulses have durations less than 1 ps in typical parametric crystals. The present theory is restricted to cases where the transverse spatial structure of the fields does not change with propagation, such as in a waveguide [9]. We have emphasized the use of the semiclassical Wigner representation as an efficient computational method for investigating squeezing in parametric amplifiers at large pump photon number and verified its applicability by comparison with the positive-P representation.

A major conclusion of this study is that the LO pulse cannot be made shorter than the inverse phase-matching bandwidth without degrading the amount of squeezing

detected. This result generalizes that of Yurke and co-workers, who showed that in the absence of dispersion, the LO pulse duration should approach zero for optimum squeezing detection. Our conclusion corrects an assumption by Blow and co-workers [28] that the optimum in the presence of dispersion is attained when the LO pulse shape matches precisely that of the signal field. The conclusion of Blow *et al.* properly arises only if the nonlinear optical process excites only a single spatial-temporal mode, leaving all other modes in the vacuum. Our work here shows that this assumption does not apply to parametric amplification of the vacuum in traveling-wave geometry.

To understand this conclusion, note that in traveling-wave OPA the down-converted field is generated with a very wide bandwidth (of the order of 1 THz) determined by the phase matching. To detect optimally a large reduction of LO shot noise, it is necessary for the spectrum of the squeezed field to be wider than that of the LO pulse, so all frequency modes of the LO can be influenced. This is possible because the squeezed field is very far from being transform limited, while the LO pulse is near transform limited. If the LO pulse duration becomes too short, however, its spectrum becomes wider than that of the squeezed field, resulting in less noise reduction.

A second major conclusion is that the action of signal and pump dispersion does not prevent the detection of very large amounts of quadrature squeezing. This can be achieved by giving the LO pulse the proper duration and phase structure. Since the group-velocity dispersion terms in the equations of motion are second order in time, they produce a quadratic phase shift across the pulses. Fortunately, the needed phase structure can be induced by passing the LO pulse through a transparent, linear medium with the proper degree of dispersion.

It is likely that the small amounts of squeezing detected so far in OPA experiments results from a combination of poor choice of pulse durations and transverse spatial effects, as discussed by LaPorta and Slusher [14] and Kim, Li, and Kumar [29]. The present treatment can be generalized to include such spatial effects; this will be reported in a future paper. We showed that more than 20 dB of squeezing is possible using group-velocity matched parametric waveguides. Using typical experimental parameters for LBO and BBO, including group-velocity mismatch and group-velocity dispersion, we also showed that waveguides of this type would generate large amounts of squeezing, in spite of the effects of group-velocity mismatch. In fact, these results predict far more squeezing than has ever been observed with bulk crystals in a traveling-wave configuration. Experiments utilizing these devices have recently been reported, but without attaining the predicted levels of squeezing [9].

We have emphasized the truncated Wigner representation as an efficient computational method for investigating squeezing in pulsed parametric amplifiers. It requires only half the number of variables as does the positive-P method. It is also more advantageous on vector processor computers as the positive-P method requires independent Gaussian noise sources to be generated for all space-time points whereas the Wigner method requires noise sources only at the medium input, if losses are neglected. Providing there are no boundary terms, the positive-P representation is an exact method since quantum noise arising from the nonlinearity is included by second-order diffusive terms in the Fokker-Planck equation. The exact Wigner representation leads to third-order derivatives in the quasiprobability evolution equation, which have been neglected here. We have demonstrated that this approximation is valid for large photon numbers and small propagation distances when calculating the squeezing spectrum. The reduced sampling error for low frequencies using the Wigner method has been noted previously by Drummond and Hardman [24]. However, the Wigner method tends to have larger sampling errors at high frequencies.

ACKNOWLEDGMENTS

M.J.W. would like to thank S. J. Carter for providing independent numerical checks in the early part of this work. M.G.R. thanks H. J. Carmichael and J. Cooper for helpful discussions.

[1] R. E. Slusher *et al.*, Phys. Rev. Lett. **55**, 2409 (1985).
[2] L. Wu, J. Kimble, J. Hall, and H. Wu, Phys. Rev. Lett. **57**, 2520 (1986).
[3] R. M. Shelby *et al.*, Phys. Rev. Lett. **57**, 691 (1986).
[4] R. E. Slusher *et al.*, Phys. Rev. Lett. **59**, 2566 (1987).
[5] T. Hirano and M. Matsuoka, Opt. Lett. **15**, 1153 (1990).
[6] P. Kumar, O. Aytur, and J. Huang, Phys. Rev. Lett. **64**, 1015 (1990).
[7] M. Rosenbluh and R. M. Shelby, Phys. Rev. Lett. **66**, 153 (1991).
[8] P. D. Townsend and R. Loudon, Phys. Rev. A **45**, 458 (1992).
[9] M. E. Anderson, M. Beck, M. G. Raymer, and J. Bierlein, Opt. Lett. **20**, 620 (1995).
[10] D. Kupiszewska and K. Rzążewski, Phys. Rev. A **42**, 6869 (1990).
[11] M. G. Raymer, P. D. Drummond, and S. Carter, Opt. Lett. **16**, 1189 (1991).
[12] B. Yurke, P. Grangier, R. E. Slusher, and M. J. Potasek, Phys. Rev. A **35**, 3586 (1987).
[13] D. T. Smithey, M. Beck, M. G. Raymer, and A. Faridani, Phys. Rev. Lett. **70**, 1244 (1993).
[14] A. LaPorta and R. Slusher, Phys. Rev. A **44**, 2013 (1991).
[15] U. M. Titulaer and R. J. Glauber, Phys. Rev. **145**, 1041 (1966).
[16] B. Schroder, Opt. Quantum Electron. **15**, 57 (1983).
[17] B. Huttner, S. Serulnik, and Y. Ben-Aryeh, Phys. Rev. A **42**, 5594 (1990).

[18] D. D. Crouch, Phys. Rev. A **38**, 508 (1988).
[19] J. Mostowski and M. G. Raymer, in *Contemporary Nonlinear Optics*, edited by G. P. Agarawal and R. Boyd (Academic, Boston, 1992), Chap. 5.
[20] P. D. Drummond and S. J. Carter, J. Opt. Soc. Am. B **4**, 1565 (1987).
[21] K. E. Cahill and R. J. Glauber, Phys. Rev. **177**, 1882 (1969).
[22] M. J. Werner and H. Risken, Phys. Rev. A **44**, 4623 (1991).
[23] P. D. Drummond and C. W. Gardiner, J. Phys. A **13**, 2353 (1980).
[24] P. D. Drummond and A. D. Hardman, Europhys. Lett. **21**, 279 (1993).
[25] D. T. Smithey *et al.*, Phys. Scr. **T48**, 35 (1993).
[26] P. D. Drummond, S. J. Carter, and R. M. Shelby, Opt. Lett. **14**, 373 (1989).
[27] M. J. Werner, Ph.D thesis, University of Queensland, 1994 (unpublished).
[28] K. J. Blow, R. Loudon, S. J. Phoenix, and T. J. Shepherd, Phys. Rev. A **42**, 4102 (1990).
[29] C. Kim, R. D. Li, and P. Kumar, Opt. Lett. **19**, 132 (1994).
[30] B. Wu *et al.*, Opt. Lett. **14**, 1080 (1989).
[31] V. G. Dmitriev, G. G. Gvrzadyan, and D. N. Nikogosyan, *Handbook of Nonlinear Optical Crystals* (Springer, Berlin, 1990).